Ray tracing simulations for crystal optics

Manuel Sánchez del Río

European Synchrotron Radiation Facility
BP 220, 38043 Grenoble-Cedex, France

ABSTRACT

A review of the physical models for crystal optics in a ray tracing program is presented. X-ray monochromators and analyzers for synchrotron radiation applications in both Bragg (reflection) and Laue (transmission) geometries can be simulated with this method. Ray tracing calculations for several high-resolution and focusing geometries are presented, demonstrating the suitability of the ray tracing method for the design and optimization x-ray crystal optics. Possible applications to study the crystal effects on partially coherent beams are also outlined.

All these systems have been modeled in the framework of the ray tracing program SHADOW. For increasing the visual and post-processing functionality of SHADOW we developed a front-end library and a Visual User Interface available from the author.

Keywords: x-ray tracing, perfect crystals, modeling, high-resolution, focusing crystals, coherence

1. INTRODUCTION

It is difficult to find a synchrotron radiation beamline operating at energies above 3 keV that does not include a crystal. Most x-ray beamlines use perfect crystals as x-ray monochromators. With the advent of the new third generation synchrotron sources, the monochromator technology has developed to deal with high heat loads, to obtain very high energy resolution and to focus the beam in narrow spots. It is essential to have access to a reliable and general modeling tool for the design, optimization and commissioning of crystal devices. This paper presents the advantages of the ray tracing method for modeling crystal optics.

The x-ray reflectivity of perfect crystals is given by the dynamical theory of diffraction.[1] The characteristics and performances of optical devices made by a combination of perfect crystals can be predicted using several graphical methods. Du Mond diagrams,[2] phase-space analysis,[3] or a combination of them, the so-called angle-position-wavelength diagram[3] are typical examples of these methods. All of them display a space of parameters (angle-wavelength for Du Mond, angle-position for the phase-space and angle-position-wavelength for the one carrying the same name) and assume that the transmitted photons are bound in a limited volume. These methods, which are useful for didactical purposes, are difficult to use for practical purposes because the graphs must be drawn considering quantitative aspects of the crystals. Some computer programs using this methods have been coded which are useful in some specific cases.

A very powerful approach to predict the performance of an optical system in general, and a crystal optical device in particular is the use of ray tracing methods. For optical systems in the visible and UV spectral range, several commercial packages are available. For synchrotron radiation applications, the code SHADOW[4] has become the *de facto* standard. In this ray tracing code, a ray is a mathematical entity fully specified by four vectors and two phases: the starting position $\vec{r}$, the momentum $\vec{k}$, the electric fields $\vec{A_\pi}$ and $\vec{A_\sigma}$ (σ and π refer to the parallel and perpendicular polarizations) and their phases ϕ_π and ϕ_σ. Therefore, the SHADOW space of variable is a *superset* of the space of variables used in any of the methods already mentioned (for instance, the angle-position-wavelength one). The source is usually created using the Monte-Carlo method to sample rays with the spatial, angular and energy distribution of the synchrotron sources, although simulation of geometrical and grid sources is also possible. Each ray of the source is traced through an optical system consisting of a number of optical elements (mirrors, gratings, crystals, etc.). The important values of beam cross sections, energy resolution, etc. are calculated by post-processing (histogramming, integration and visualization) the resulting SHADOW files.

Other author information:
Email: srio@esrf.fr; Telephone: +33-476 882 513; Fax: +33-476 882 160

Two crystal models are available in SHADOW: mosaic and perfect crystals. The mosaic crystal model is described in Ref. 5 and some calculations compared with experimental data are presented in Ref. 6. In this paper we only refer to perfect crystals, which are indeed the most extensively used. The SHADOW model for perfect crystal diffraction is conceptually very simple. In the diffraction process, the momentum of the ray is changed following two assumptions: i) the elastic scattering, and ii) the continuity of the tangential components of the wave vectors through the surface. In addition, the electric fields are modified according to the equations of the dynamical theory of the diffraction. This paper demonstrated that with only these three general hypotheses it is possible to simulate a large number of optical devices consisting in one or several perfect crystals arranged in different geometries and configurations.

All the simulations presented in this paper have been performed with the SHADOW code. In addition, we developed a library of functions written in IDL[7] to improve the graphical and post-processing functionality of SHADOW. We found that IDL can be a nice and comfortable interface to communicate with SHADOW, prepare its input data, create macros to automatize SHADOW loops, perform highly sophisticated 2D and 3D graphics, etc. In addition, the library modules have been integrated in a complete Visual Graphical Interface (SHADOWVUI), which is available free of charge for research institutions as an *extension* of the XOP[8] package.

2. THEORETICAL MODEL

In the ray tracing program, the modeling of the diffraction phenomenon by a perfect crystal takes place in two steps. The first one calculates the change of direction of the ray in the diffraction process using only geometrical concepts that any ray tracing code must include. This is the so-called *geometrical method*. The second one includes the physical collective phenomena that take place inside the crystal. Thus, only the rays arriving to the crystal forming an angle with respect to the crystal planes close to the Bragg angle will be reflected. The code treats the crystal as an entity that receives a ray with electric field $\vec{A}$ and returns the ray with a modified electric field $\vec{A}\,R$ where R is the crystal reflectivity given by the dynamical theory of diffraction. This is the *physical model*.

The geometrical and physical models described here are discussed for monochromatic incident radiation, but these equations are applied individually to each ray in the beam. Since different rays may have different wavelengths, we can deal with polychromatic or white beams with SHADOW. In other words, our *beam* is a collection of independent *rays*, in which each ray has an assigned wavelength, so that the whole collection of rays (i.e., the beam) is polychromatic or monochromatic, depending on the case studied.

2.1. The geometrical model

The change in the direction of a *monochromatic beam* diffracted by a perfect crystal (Laue or Bragg) can be calculated supposing elastic scattering in the diffraction process:

$$|\vec{k}_1| = |\vec{k}_2|, \tag{1}$$

and using the boundary conditions at the crystal surface

$$\vec{k}_{2,||} = \vec{k}_{1,||} + \vec{G}_{||}, \tag{2}$$

where $\vec{k}_1$ and $\vec{k}_2$ are the incident and exit wave vectors (outside the crystal), $\vec{G}$ is the reciprocal lattice vector, and $||$ refers to the component parallel to the crystal surface. From these equations we obtain the angular direction of the outgoing photons:

$$\sin\theta_2 = \sin\theta_1 + (\lambda/d_{hkl})\sin\alpha, \tag{3}$$

θ_1 and θ_2 being the incoming and outcoming angles, respectively, measured respect to the crystal surface. λ is the photon wavelength, d_{hkl} the interlattice distance (d-spacing) and α is the asymmetry angle ($\alpha = 0$ for symmetrical Bragg case and $\alpha = 90^\circ$ for symmetrical laue case). The emergent ray direction θ_2 is a function of the incident angle and of the photon energy. This energy dependence exists for all cases except for the symmetrical Bragg, where $\alpha = 0$ and then $\theta_1 = \theta_2$ (specular reflection). Therefore, the diffraction by any Laue crystal and any asymmetric Bragg crystal is a typical dispersive process. Specular reflection on the Bragg planes does not exist in general. Specular

reflection only exists for any crystal in the particular case that the incident ray exactly fulfills the Bragg kinematical law.

Notice that the above equations describing the change in direction of the monochromatic collimated beam (or a ray) are equivalent to considering a diffraction grating created by the termination of the Bragg planes ($d_{grating} = d_{hkl}/\sin\alpha$). For the case of a perfect flat surface (symmetrical Bragg case, $\alpha = 0$), the period of this grating is infinity and no scattering occurs so that the reflection is specular ($\vec{G}_{||} = 0$). In all the other cases, the intersection of the Bragg planes with the crystal surface forms a grating structure of ruling $d_{grating}$ which scatters the incident ray into another direction which depends also on its energy.

2.2. The physical model

The diffraction profile of a single perfect parallel-sided crystal of thickness t in Bragg (or reflection) and Laue (or transmission) geometries can be calculated as:

$$R^2_{bragg} \equiv \frac{1}{|b|}\frac{I_H}{I_0} = \frac{1}{|b|}\left|\frac{x_1 x_2 (c_1 - c_2)}{c_2 x_2 - c_1 x_1}\right|^2 \quad ; R^2_{laue} \equiv \frac{1}{|b|}\frac{I_H}{I_0} = \frac{1}{|b|}\left|\frac{x_1 x_2 (c_1 - c_2)}{x_2 - x_1}\right|^2 , \tag{4}$$

where I_H is the intensity of the external diffracted wave, I_0 is the intensity of the incident wave, $c_1 = exp(-i\phi_1 t)$, $c_2 = exp(-i\phi_2 t)$, $\phi_1 = 2\pi k\delta'_0/\gamma_0$, $\phi_2 = 2\pi k\delta''_0/\gamma_0$, γ_0 (γ_h) is the direction cosine of the incident (diffracted) wave and the other quantities are defined as:

$$\begin{pmatrix} \delta'_0 \\ \delta''_0 \end{pmatrix} = \frac{1}{2}\left(\Psi_0 - z \pm \sqrt{qP^2 + z^2}\right) \quad ; \quad \begin{pmatrix} x_1 \\ x_2 \end{pmatrix} = \frac{-z \pm \sqrt{qP^2+z^2}}{P\Psi_{\bar{H}}} \quad ; \tag{5}$$

$$z = \frac{1-b}{2}\Psi_0 + \frac{b}{2}\tau \quad ; \quad \tau = \frac{1}{|\vec{k}_1|^2}\left[|\vec{G}|^2 + 2\vec{k}_1 \cdot \vec{G}\right] \quad ; \tag{6}$$

$q = b\Psi_H\Psi_{\bar{H}}$, P is the polarization factor, Ψ_H is the Fourier component of the electrical susceptibility Ψ_0 and $b = \gamma_0/\gamma_h$ is the asymmetry factor.

Note that this formulation is valid for plane crystals. When a perfect crystal is elastically bent, the diffracted beam is modified with respect to the plane case because of two reasons. The first is the bent geometry, which generates an angular distribution of the entrance angle of the rays with respect to the crystal surface along the beam footprint. This angular distribution causes changes in the total diffracted intensity. This effect can be can be analysed by ray tracing, as shown in the next paragraphs. The second reason is that, when the crystal curvature radius is "small enough", the crystallographic atomic planes suffer a distorsion and the local reflectivity of the crystal at any point of its surface varies drastically. In other words, the mechanical tensions related to the bending entail a misalignment between the atomic planes causing, in general, an enlargement of the diffraction profiles. Several models have been proposed for calculating the diffraction profiles for bent crystals[9] and their integration in SHADOW is under study. In the following, we will assume in the case of bent crystals that the crystal curvature does not produce any distorsion in the diffraction profile respect to the case of flat crystal. In other words, the crystal behaves *locally* (i.e., on a very small area on its surface) as a flat crystal, in order to assure that the Zachariasen theory is applicable.

3. BENCHMARK TESTS

3.1. Phase space

The use of the phase space method for synchrotron radiation beamline design has been inherited from machine physics. It consists in studying the evolution of the photon beam in the plane position-angle, either in the horizontal plane (x, x') or in the vertical one (z, z'). A perfect crystal modifies the phase space plot affecting the diffraction plane. Supposing that the diffraction plane is vertical, the crystal, in general, modifies the divergence space due to the Eqs. 2. But the area of the diagram must be conserved as required by the Liouville theorem (or its analogous version, the Smith-Helmholtz invariant). This is explained in Ref. 3, where the authors also analyze the 3-dimensional space (z, z', λ) called position-angle-wavelength space.

The conservation of the phase-space volume in the diffraction process is always verified in the SHADOW calculations. After the diffraction process, the rays form a cloud of points in any chosen parameter space. As any ray

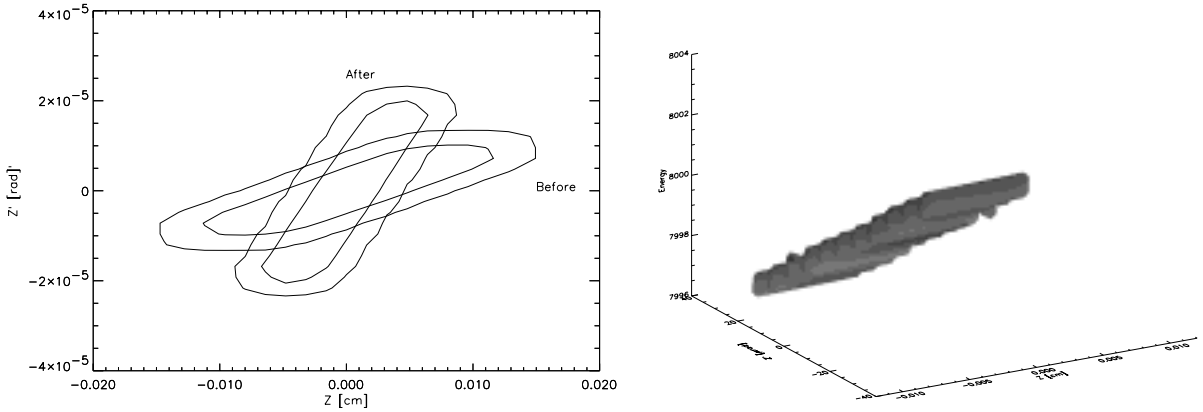

Figure 1. *Left:* Change in phase space (z, z') of a photon beam of 8 keV created by a linear (0.1 mm) and divergent (20 μrad) source. An asymmetric ($\alpha = 5^\circ$) $Si < 1,1,1 >$ crystal in Bragg geometry was used. The contours represent the FWHM and the FW10The two plots corresponts to the phase space before diffraction and after diffraction. *Right:* position-angle-wavelength space before the diffraction, for the same system. The roughness in the volume is due to unphysical artifacts left by the triangulation and interpolation done to create the volume plot.

has an intensity assigned $I = |\vec{A}_\sigma|^2 + |\vec{A}_\pi|^2$, the parameter space consists in a volume with a given intensity density. The total intensity of the diffracted beam is just the Stieltjes integral of this density over the hyper-volume of the variable space. An example of the (z, z') phase-space is shown in Fig. 1, where a monochromatic beam of 8 keV created by a linear and divergent source in z is diffracted by an asymmetric crystal (asymmetry angle $\alpha = 5^\circ$) of 8 keV. We have plotted the contour curves of the intensity density in the (z, z') phase space in a plane perpendicular to the beam immediately after the crystal. The same plot may be done as a function of the parameter space before the diffraction, in order to see the change produced by the diffraction process. Fig. 1a is a good example of how the shape of the phase space volume changes while conserving the total volume unchanged. Fig. 1b shows the position-angle-wavelength graph for the same system. It is clearly demonstrated that the density of intensity dependens on the energy. This fact is in agreement with the position-angle-wavelength graph in Ref. 3 (Fig. 16).

3.2. Du Mond diagrams

This graphical analysis method was proposed by Du Mond[2] in 1937 for studying the resolution of x-ray crystal systems with several crystal reflections. It is very useful to understand and analyze the combination of identical or different crystals in both non-dispersive [$(+n, -n)$ for identical crystals and $(+n, -m)$ for different ones) and dispersive $(+n, +m)$] configurations. It allows to display multi-crystal systems sequentially and can also explain the effect of an asymmetry in the crystal cut.

The Bragg law gives the dependency of the wavelength λ versus the angle θ. The maximum of the diffraction corresponding at a given Bragg angle θ_0 is $\lambda_0 = 2d_{hkl} \sin\theta_0$. When a white beam of a given divergence Δ_{src} impinges on the crystal, it produces a dispersion of the Bragg angle on the crystal surface with the same value Δ_{src} (supposing the crystal is flat) centered in θ_0. Therefore, different wavelengths will be reflected, each one corresponding to a different incident angle. The spectral resolution of the reflected beam can be easily calculated considering the pendent m of the $\lambda(\theta)$ plot at λ_0:

$$m = \frac{d\lambda}{d\theta} = 2d\cos\theta_0 \;\; ; \frac{\Delta\lambda}{\lambda_0} = \frac{\Delta E}{E_0} = \Delta\theta \cot\theta_0, \tag{7}$$

and in our case $\Delta\theta = \Delta_{src}$ because the beam divergence is the only component of indetermination in θ.

Du Mond, arguing that a given λ_0 reflection can be obtained not only by its Bragg angle θ_0 but also by other angles close to it (manifested in the diffraction profile or in the Darwin width), affirms that λ and θ must be treated as independent variables. The x-ray intensity is a function of both λ and θ regarded as independent of each other. The effect on the (λ, θ) graph is that the line $\lambda(\theta)$ defined by the Bragg law becomes a band of thickness (in fact

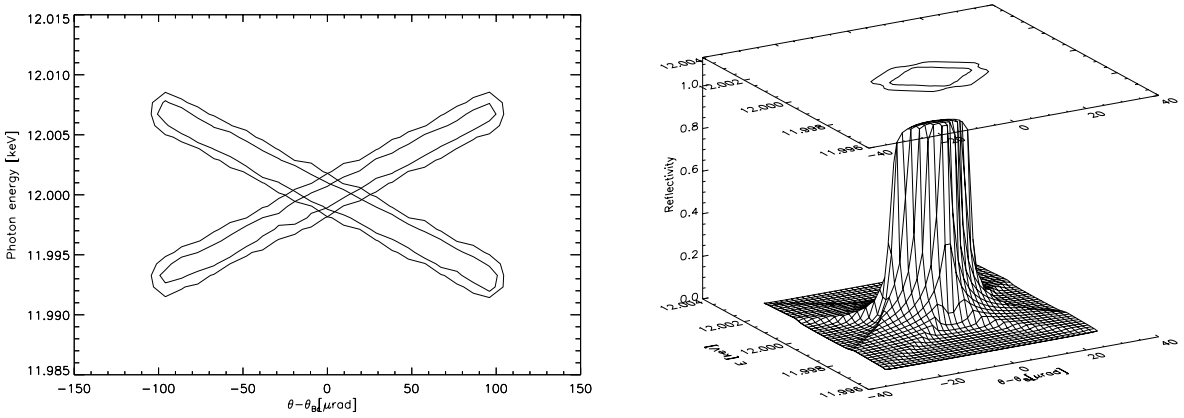

Figure 2. *Left:* Du Mond diagram $E(\theta)$ for two antiparallel $(+,+)$ $Si < 1,1,1 >$ crystals at 12 keV. Each band corresponds to a given crystal. The contours correspond to the FWHM (internal contour) and FW10%M (external one).
Right: Intersection plot of the two bands.

the $\lambda = cte$ section) equal to the Darwin width. This band has a different width for different θ values (because the Darwin width changes as a function of θ) and has an intensity profile with follows the diffraction profile. It is generally a good approximation to assume that the band has a constant thickness in the neighborhood of θ_0 and its intensity profile is flat (i.e., the diffraction profile is a box distribution). Under these conditions, the diffracted beam intensity is proportional to the area of the band under the limits $\Delta\theta$.

The Du Mond diagram is very powerful to understand crystal combinations. A system formed by two parallel identical crystals $(+,-)$ will be represented by two bands, one on the top of the other. The result is the intersection between these two bands, which is exactly the same as the band of the first crystal. If one crystal is misaligned, the intersection area becomes narrower, thus the transmitted intensity decreases. If the misalignment is larger than twice the Darwin width, the intersection is zero. Thus, no transmitted beam is found. In a $(+,-)$ system (also called non-dispersive), the spectral resolution depends on the beam divergence and band width:

$$\frac{\Delta\lambda}{\lambda_0} = \frac{\Delta E}{E_0} = (\Delta_{src} + \omega_D)\cot\theta_0 \tag{8}$$

A system formed by two identical antiparallel crystals $(+,+)$ shows that if one increases the θ angle for the first crystal respect to the Bragg angle θ_0, the grazing angle on the second crystal is reduced. In the Bragg law plot $\lambda(\theta)$ the first crystal stands in a point of the upcoming branch of the sinusoid (positive pendent) whilst the second one stands on a descendent branch (negative pendent). This results in crossing bands in the Du Mond diagram. Is is easily verified that spectral resolution produced by this system does not depend on Δ_{src} (considering always that $\Delta_{src} >> \omega_D$) but only on ω_D. Under these conditions, the spectral resolution of the $(+,+)$ system (also called dispersive) is always better than the $(+,-)$ case.

When considering asymmetrically cut crystals, more than two (λ and θ) independent variables are required to represent completely the intensity of the reflection. This is due to the fact that these crystals make a change in the divergence as shown above. Thus, the accepted source divergence and the Darwin width calculated versus incident angle must be transformed to the outcoming angle. Therefore two bands are necessary for each crystal. This is explained in Ref. 3.

Du Mond diagrams can be easily done with ray tracing. In fact, it is also possible to consider the intensity profiles of the bands. An example is shown in Fig. 2 where one can see the effect of a dispersive system formed by two identical $Si < 1,1,1 >$ crystals set to reflect 12 keV photons.

3.3. Some analytical formulas for crystal optics

We have stated that a crystal behaves like a grating with a ruling produced by the truncation of the Bragg planes with the crystal surface. This equivalence refers only to the changes introduced by the crystal in the incident wavefront. This assumption permits to write the formulas that describe the *focusing of monochromatic beam* in the same way that is done for gratings[10]:

$$\frac{1}{p}+\frac{1}{q}=\frac{\sin\theta_1+|\sin\theta_2|}{R_s}\ ;\ \frac{\sin^2\theta_1}{p}+\frac{\sin^2\theta_2}{q}=\frac{\sin\theta_1+|\sin\theta_2|}{R_t}\ , \tag{9}$$

where p is the distance source-crystal, q is the distance crystal-focus, R_s (R_t) is the radius to focus in the sagittal (tangential) plane and $\theta_1=\theta_0+\alpha$ and $\theta_2=\theta_0-\alpha$, as required by the Bragg law. In the case that the incident beam is collimated (incident plane wave) one should put $p=\infty$ in the above formulas. Likewise, to create collimated diffracted beams one should use $q=\infty$. The same formulas are obtained in Ref. 11.

In the particular case of Bragg symmetrical crystals, $\theta_1=\theta_2=\theta_0$ and the Eqs. 9 reduce to the well known ones:

$$\frac{1}{p}+\frac{1}{q}=\frac{2\sin\theta_0}{R_s};\quad \frac{1}{p}+\frac{1}{q}=\frac{2}{R_t\sin\theta_0}. \tag{10}$$

The dimension of the focal spot s_2 is related to the source size dimensions s_1 by the magnification factor M (without taking into account spherical aberrations):

$$s_2=s_1M=s_1\frac{q}{p}\equiv s_1\ (q:p). \tag{11}$$

It is noteworthy to stress that the focal dimension calculated in this manner is only valid for monochromatic incident beams. If the incident beam is polychromatic or white, the crystal itself will select an energy bandwidth, and although this energy bandwidth could be small, it produces *chromatic aberrations*. This is due to the fact that crystals, in general, are dispersive systems (like gratings) that focus different wavelengths in different points smearing the focal spot. These chromatic aberrations exist in all cases except the Bragg symmetrical case, because this system, as mentioned above, behaves as a non-dispersive system (mirror). The energy bandpass is therefore determinant for the spot dimensions. An analytical formula for this broadening of the focal spot using asymmetric crystals due to the chromatic aberrations is given in Ref. 12.

In order to calculate the spectral bandpass produced by a crystal, we have seen that one should use $(\Delta E)/E=\Delta\theta\cot\theta_0$. The angular indetermination has three different origins: i) the Darwin width ω_D (which for asymmetrically cut crystals is related to the symmetrical Darwin width ω_0 by the asymmetry factor $\omega_D=\omega_0/\sqrt{b}$, ii) the divergence seen by the crystal which is mainly due to the angular dispersion along the intersection of the beam with the crystal surface Δ_{geom} (in the case of flat crystals it becomes Δ_{src}), and iii) the source size as seen from the crystal position Δ_{ss}. If we assume that the Darwin width and the divergence seen by the crystal have gaussian profiles (which is not true, but is generally considered like that), one can add them in quadrature and write Eq. 7 as:

$$\frac{\Delta\lambda}{\lambda_0}=\frac{\Delta E}{E_0}\approx\sqrt{\omega_D^2+(\Delta_{geom}+\Delta_{ss})^2}\cot\theta_0=\sqrt{\omega_D^2+\left[\left(\frac{p}{R\sin\theta_1}-1\right)\Delta_{src}+\frac{s_1}{p}\right]^2}\cot\theta_0, \tag{12}$$

where R is the crystal curvature and the effects of the beam penetration depth inside the crystal have been neglected. Some plots of this equation versus R are in Ref. 13, showing also the good agreement of points calculated with SHADOW. The best energy resolution (intrinsic resolution) is obtained when Δ_{geom} and Δ_{ss} are zero. In this case $\Delta E/E$ is only dependent on the product of the Darwin width ω_D times $\cot\theta_0$, which is independent on E.

4. HIGH RESOLUTION MONOCHROMATORS AND ANALYZERS

High resolution crystal devices minimize the Eq. 12 respect to one or several of its dependent parameters. If one wants to minimize $\cot\theta_0$ it is necessary to design devices using crystals in normal or quasi-normal incidence ($\cot\theta_0$ can be of the order of 10^{-3} or 10^{-4}) as discused later. If one wants to minimize the square root of Eq. 12, one should work with point sources ($s_1/p = 0$) and then try to work in conditions that the Δ_{geom} term is zero. This can be achieved in several ways: i) using collimated incident beams ($\Delta_{src} = 0$), ii) working in the Rowland condition $p/(R\sin\theta_1) = 1$, and, iii) using dispersive crystal combinations, that make $\Delta_{geom} = 0$, as shown before. A minimization of the ω_D term can be achieved using high order reflections or asymmetric systems, where the angular acceptance is changed respect to the symmetrical crystal by a factor of $1/\sqrt{b}$.

In this section, several high resolution monochromators and devices used in synchrotron beamlines are summarized and some ray tracing results are presented.

4.1. Collimating pre mirror

It is well known that in a typical two-crystal monochromator the resolution is improved by reducing the divergence of the beam with entrance slit. This goes in detriment of the transmitted flux. The resolution can be improved *without loosing in transmitted flux* by collimating the entrance beam using a parabolic mirror (the mirror is considered to reflect ideally). In most cases, a cylindrical mirror is used instead of a parabolic (ideal) one because it is easier to manufacture and align, and approximates very well the parabolic surface. The resolution will depend on the residual divergence left by the collimating mirror due to inevitable figure and slope errors. Table 1 shows resolution and flux results for different collimating mirror surfaces, demonstrating that the cylindrical mirror is a good solution for the case considered (the ESRF bending magnet source, at 10 keV, using a double $Si < 1,1,1 >$ crystal monochromator).

Table 1. Ray tracing results for a double crystal monochromator operating at 10 keV with a collimating mirror placed 20 m from the source and 10 m before the monochromator. The mirror grazing angle is 3 mrad. The source is the ESRF bending magnet with source size FWHM 85 μm and source divergence FWHM 185 μrad. The table shows the energy resolution (FWHM), the transmitted intensity I (arbitrary units) and the beam divergence (FWHM) of the diffracted beam. The results show that the use of a cylindrical mirror is adequate in this configuration because it gives the same results than the ideal parabolic surface. Note the degradation of the resolution due to the residual divergence left by the slope error in the mirror (slope errors are considered with the model described in Ref. 14). Note also that the flux delivered by all these systems is the same. The reflectivity of the mirror has been considered perfect. All the optical surfaces are considered of infinite dimensions. The error value refers to the standard deviation calculated considering the results of ten SHADOW runs with 5000 rays each.

Mirror	ΔE[eV]	I	$\Delta\theta[\mu$rad]
No mirror	8.47±0.99	1008 ±38	158±24
Parabolic	1.27±0.05	1004 ±20	3.9±0.3
Elliptical	1.27±0.05	1004 ±20	3.9±0.3
Cylindrical	1.28±0.06	1002 ±18	4.4±0.3
Cylindrical+1 arcsec slope	1.44±0.15	1000 ±20	20.7±2.9
Cylindrical+2 arcsec slope	2.33±0.12	1008 ±18	38.5±3.6

4.2. Rowland bending

When the crystal surface is bent, the dispersion on the Bragg angle formed by the intersection of the incoming beam with the crystal surface is different than the beam divergence. In other words, $\Delta_{geom} \neq \Delta_{src}$. In order to make $\Delta_{geom} = 0$, even working with a divergent source, one should make $s/(R\sin\theta_1) = 1$, which is achieved in the Rowland condition. In the case of symmetric crystals in reflection mode, the Rowland condition is satisfied in the $p = q$ condition, i.e., in 1:1 magnification. In the case of asymmetric crystals, the Rowland condition does not correspond to 1:1 magnification. This is discussed in Ref. 13.

It is possible to increase the resolution of a crystal by bending it following the Rowland circle. One could try to apply this rule to a double crystal monochromator, and try to increase the resolution by bending the first crystal.

Let us consider a double crystal monochromator with symmetrical crystals (similar arguments can be applied to asymmetric systems), it is shown in Table 2 that the resolution is increased for any bent-flat system, but the transmitted flux is drastically reduced respect to the flat-flat system. This is because in a bent-flat system, each ray impinges on the first crystal with an angle different to the one for the second crystal. The transmitted intensity can be improved by bending the second crystal with the same curvature but opposite convexity than the first one. This system is non-dispersive and its transmitted flux is comparable to the flat-flat system, but the focalization is lost. The fact that two non identical surfaces give a dispersive effect can be used for improving the resolution in non-Rowland configuration. A monochromator with a first bent crystal to focus in 1 : 3 magnification configuration and a second flat crystal gives better results in terms of resolution than the flat-flat configurations and are slightly worse than the Rowland one.

Table 2. Ray tracing results for a symmetric double crystal monochromator operating at 10 keV for different crystal shapes: flat-flat, bent(Rowland)-flat, bent(out-Rowland)-flat and two bent(Rowland) crystals with different convexity. The table shows the intensity (in arbitrary units) after the first crystal I_1 and after the second crystal I_2, as well as the energy resolution FWHM ΔE_1 and ΔE_2 after the first and second crystals, respectively. The source is the ESRF bending magnet with source size FWHM 85 μm and source divergence FWHM 185 μrad. The monochromator is placed at 30 m from the source. All the optical surfaces are considered of infinite dimensions. The error value refers to the standard deviation calculated considering the results of ten SHADOW runs with 5000 rays each.

System	I_1	I_2	ΔE_1[eV]	ΔE_2[eV]
flat-flat	413±14	307±12	8.92±0.55	8.71±0.69
Rowland(1:1)-flat	414±25	65±9	1.44±0.06	1.23±0.24
Rowland(concave)-Rowland(convex)	399±12	296±10	1.44±0.07	1.32±0.06
Out-Rowland(1:3)-flat	408±18	36±3	8.2±0.9	2.1±0.5

4.3. Normal incidence

The resolving power described in Eq. 12 can be reduced up to three orders of magnitude if one choses a Bragg angle close to the normal incidence position. This is due to the dependence on $\cot\theta$, which is shown in Fig. 3a. Although this geometry is not convenient for many monochromator applications, it has been used successfully for monochromators and analyzers in beamlines dedicated to inelastic scattering. The combined use of normal incidence and a bent crystal in the Rowland circle allowed experimental energy resolution of $\Delta E/E = 2\ 10^{-8}$ (see Refs. 15 and 16).

The validity of the dynamical theory of x-ray diffraction near 90° has been studied in several papers (see Ref. 17 and references therein). The authors affirm that some approximations normally done are not valid close to 90°. We should point out that these approximations regard the parameter τ in Eq. 6 that describes the separation of the incident angle respect to the Bragg angle. In SHADOW, the Eq. 6 with no approximations has been coded, thus the validity of the calculations is guarantied in the normal incidence regime.

We have modeled the system described in Ref. 15. The system consists in a $Si < 13, 13, 13 >$ crystal with surface following the Rowland circle with a radius $R = 250$ cm. The crystal is built by a high number of small crystals that follow the spherical surface. There is no stress in the lattice planes and the dynamical theory for flat crystals can be locally applied, as done by SHADOW. The energy scan is done by changing the crystal temperature, which changes the d-spacing due to the thermal expansion. This technique is also used in the simulations in Ref. 17. We used a Bragg angle of 89.98° corresponding to a photon energy of about 25.7 keV (that depends on the exact numerical value of the lattice parameter), and a Debye-Waller factor e^{-M} =0.13. More accurate Debye-Waller factors for other reflections are given in Ref. 18. The diffraction profile has a FWHM of 38 μrad, and a peak value of 0.60. A plot in the divergence space (x', z') made using SHADOW's results is presented in Fig. 3b. The calculated energy resolution is 0.28 meV. The ray tracing method permits to study changes in the radius of curvature, surface errors, finite source size, etc. As an example, if we use a Debye-Waller of 0.2 instead of 0.13, the resolution becomes 0.45 meV, a closer value to the experimental one (0.5 meV). The calculated energy resolution of a system using high reflections is very dependent on the Debye-Waller value used.

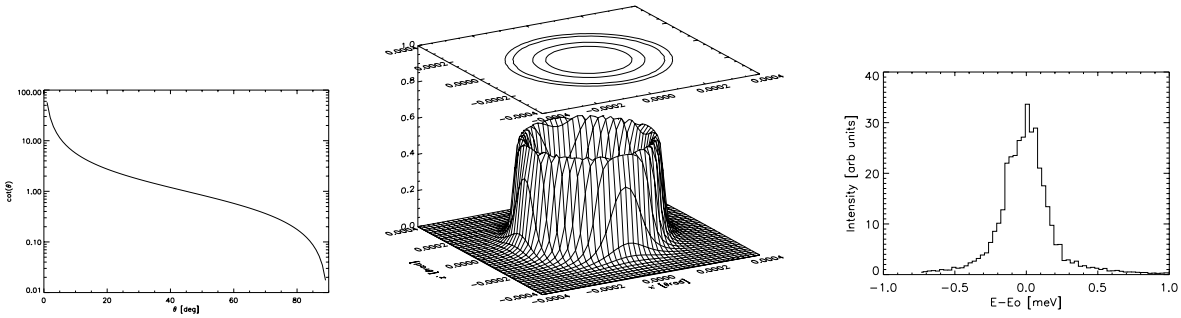

Figure 3. *Left:* Function $\cot(\theta)$.
Center: Diffracted intensity plot versus horizontal and vertical divergences. A point monochromatic (E=25702.3 eV) source has been used and a flat crystal is positioned in perpendicular to the beam. Thus, the $(x', z') = (0, 0)$ value corresponds to the normal incidence. The radial section of this ring is the reflectivity profile.
Right: Histogram of the diffracted intensity versus photon energy produced by a $Si < 13, 13, 13 >$ analyzer with curvature radius R=250 cm, giving a resolution of 0.28 meV FWHM. We used a point white source located in the Rowland circle.

4.4. Multicrystal dispersive systems

Another approach to obtain high energy resolution is to use two or more crystals arranged in the dispersive $(+, +)$ configuration. We have seen that the energy resolution using this configuration depends on ω_D, and the Δ_{geom} term is zero. By using four crystals, it is possible to obtain a diffracted beam parallel to the incident one (very suitable for synchrotron beamlines) and playing with the asymmetry angles one can beam a monochromator that accepts the full angular divergence of the incident beam and match the angular acceptance between crystals. A nested channel cut monochromator based on this idea was proposed by Ishikawa[19] *et al.* and is in use at the nuclear x-ray scattering beamlines at both ESRF[20] and APS[21] facilities. These monochromators are designed to work at the neighborhood of the photon energy corresponding to a given nuclear resonance. We have modeled the system described in Ref. 22 consisting in a nested $(+m, +n, -n, -m)$ configuration using asymmetric $Si < 10, 6, 4 >$ reflections ($\alpha = -20°$ and $20°$ for the first and fourth crystals, respectively) for the m reflections and symmetrical $Si < 4, 2, 2 >$ for the n ones. The monochromator is designed to work at the nuclear resonance in ^{57}Fe at 14413 eV. Using Debye-Waller factors of e^{-M} =0.91 and 0.55 for the $< 4, 2, 2 >$ and $< 10, 6, 4 >$ reflections, respectively, we obtained from SHADOW a resolution of ΔE=6.3 meV and an accepted divergence of 20.3 μrad (values of 6.7 meV and 22 μrad are given in Ref. 22). Another monochromator consisting in two highly asymmetric crystals ($Si < 9, 7, 5 >$ reflections, $\alpha_1 = -75.4°$, $\alpha_2 = 75.4°$ and $\theta_0 = 80.4°$) has been built and tested by Chumakov[23] *et al.* which delivered an experimental resolution of 1.65 meV at 14413 eV (1.57 meV theoretically, after the same reference). The SHADOW results shown a resolution of 1.2 meV FWHM and accepted divergence of 3.5 μrad FWHM using a Debye-Waller factor of 0.56. We have seen that the values calculated by SHADOW are always consistent with theoretical and experimental ones. Because the energy resolution and divergence calculated values are obtained from the FWHM of the corresponding intensity histograms, some errors are expected due to statistical errors in calculations. Ray tracing runs must be repeated several times in order to obtain statistical values of the errors, as done in Tables 1 and 2. The numerical values of the Debye-Waller factor may affect considerably the results, as mentioned above. It is also possible from the SHADOW output files to build Du Mond-like diagrams of the same type as presented in Ref. 21. The Fig. 4 shows the results of the two monochromators analyzed here. Slightly improved versions of these monochromators are described in Ref. 20.

5. FOCUSING OPTICS

5.1. Polychromatic focusing with flat Laue crystals

Perfect crystal in Laue configurations can be used effectively for x-ray monochromators dealing with high load. Flat Laue crystals show an interesting focusing effect when the incident beam is white and divergent. The study of this

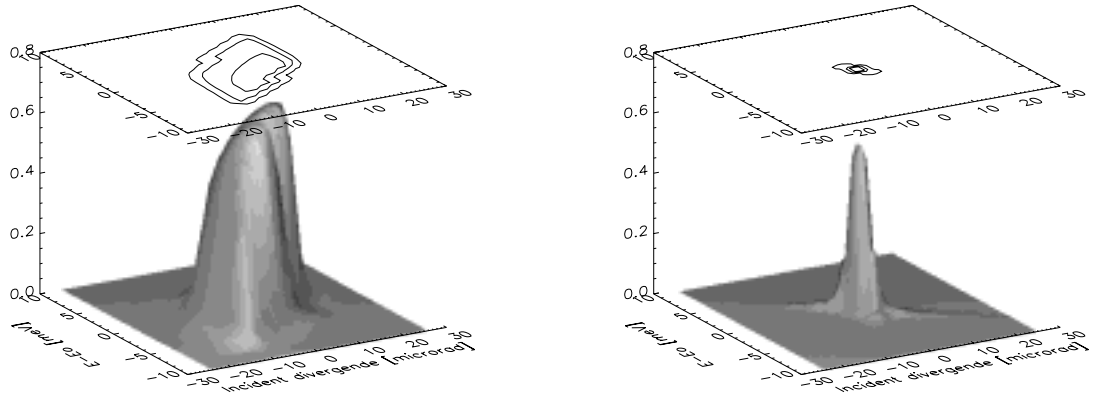

Figure 4. *Left:* Diffracted intensity versus photon energy and incident angle delivered by the four-crystal nested monochromator (see text).
Right: Same for the two highly asymmetric crystal monochromator.

effect was at the origin of the development of the Laue crystals model in SHADOW,[24] and the results agree with experimental data obtained using a diamond monochromator at ESRF.[25] These results are summarised here.

A system consisting in an undulator source (sizes 957 and 212 μm in the horizontal and vertical planes, respectively) and divergences of 40 μrad (H) and 212 μrad (V), and a double crystal almost-non-dispersive asymmetric-Laue-Diamond-$< 1,1,1 >$ and symmetric-Bragg-Ge-$< 2,2,0 >$ was used. The beam cross section after diffraction was measured and calculated at different planes downstream the monochromator for different values of an entrance slit (thus entrance beam divergences). Both the calculated (Fig. 5a) and experimental results showed that with wide entrance slits the beam after diffraction reduces its cross section as the distance to the diamond crystal increases, and with intermediate or small slits the cross section decreases. It was also found that the beam size is larger for the case where it decreases with distance than where it increases.

This effect can be illustrated as done in Fig. 5b. From this picture one can see that a polychromatic beam with divergence larger than the Darwin width globally converges after diffraction but each individual photon energy (i.e., a monochromatic beam) is reflected only into a small angular acceptance (Darwin width) and the reflected beam is also divergent because of Eqs. 2. The Laue crystal separated spatially and angularly the rays of different photon energy of the diffracted beam, which evolve in a different manner. Therefore, the resulting cross section can be seen as a total contribution of individual monochromatic beams of energy E filling the ΔE interval accepted by the monochromator. By reducing the diffracted beam energy bandwidth by closing the slit, some of the components of the total beam will be revealed, and the total beam size and evolution may change. In fact, when the ΔE interval of the diffrected beam is smaller than the intrinsic resolution of the crystal, the diffracted beam evolves divergently. Converseley, if ΔE is much larger than the intrinsic resolution, each individual energy component evolves divergently, but all the monochromatic beams cross in a given position, making the overall diffracted beam apparently convergent. In order to benefit from the pseudo focusing effect of these crystals in beamline configuration, one has to use a divergence much larger than the diffraction profile width, which is not the case when using undulator radiation from low-emittance third generation storage rings.

The use of any Laue crystal (symmetrical or asymmetrical) induces in the beam the pseudofocusing effect which must be considered when inserting other focusing optics (i.e., mirrors or multilayers) or when calculating the curvature radii for bent Laue crystals. The Laue crystals are dispersive devices in the sense that Eq. 2 must be used to calculate the divergence of the diffracted beam, thus creating chromatic aberrations.

5.2. Off-rowland mounting: dispersive EXAFS

In section 4.2, we obtained high resolution by minimizing Δ_{geom} in Eq. 12. Now we want to do the contrary: to increase the energy bandwith by doing $p/(R\sin\theta_1) >> 1$ we will be out of the Rowland configuration. This scheme is used for dispersive EXAFS beamlines,[26] where a synchrotron beam is diffracted by a crystal bent in such a manner

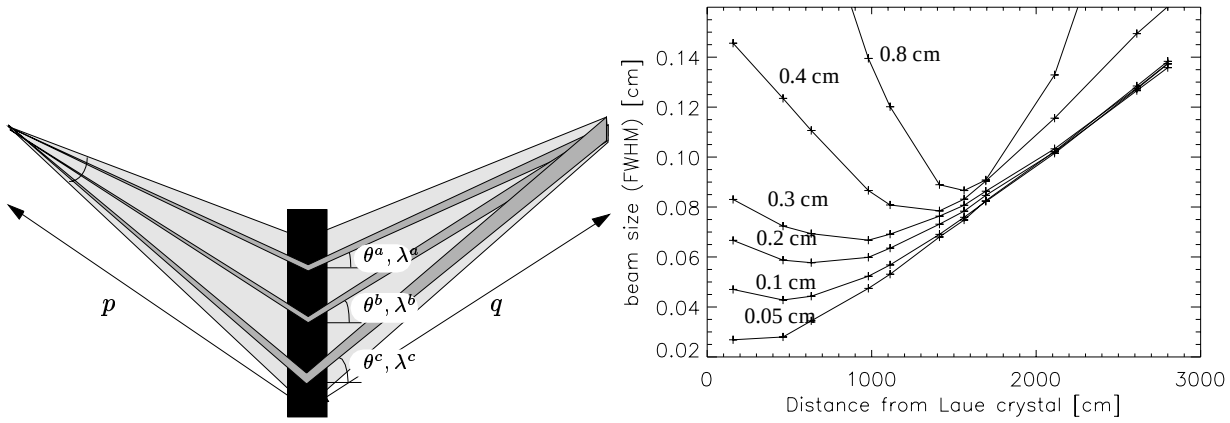

Figure 5. *Left:* Schematic representation of the pseudofocusing effect of a Laue crystal for a white divergent beam. The selective reflections on the Bragg planes produces a pseudo-focus when the quasi-monenergetic divergent beams cross.
Right: Ray tracing results of the Laue-Bragg monochromator system. The different curves correspond to different values of entrance slit aperture. One can see that for large slit apertures the diffracted beam converges to a minimum, and for small apertures the beam is always divergent.

that the energy bandwidth is enough to cover a typical EXAFS spectrum (500-1000 eV). The sample is placed in the focal position of the crystal and a multielement position sensitive detector records, downstream from the sample, the transmitted intensities (each energy will correspond to a different spatial position). For an asymmetric crystal, the focal position q is related to the crystal radius R and source position p by:

$$\frac{\sin\theta_1}{p} + \frac{\sin\theta_2}{q} = \frac{2}{R} \tag{13}$$

This equation gives the *polychromatic focus* (the point where the different rays with different energies are crossing) and is different from the monochromatic focusing Eq. 9. Eq. 13 assumes specular reflection on the Bragg planes. In the case of symmetrical crystals, Eq. 13 reduces to Eq. 10. It is clear that the size of the polychromatic focus cannot be smaller than the beamsize of any of its monochromatic components at the focal position. This is illustrated in Fig. 6, where a $Si < 1,1,1 >$ bent (R=9.88 m) crystal has been placed 40 m far from a point divergent source. The beam profiles in the diffraction planes have been calculated at two positions q: at the monochromatic focal position q_t (calculated using Eq. 9) and at the polychromatic focal position q_e (following Eq. 13). One can see that although the width of the monochromatic lines is smaller at q_t, the overall width (polychromatic focus) is smaller at q_e.

When calculating EXAFS dispersive systems with SHADOW a problem of low statistics could arise if the fully white source is used. For those cases, either a SHADOW loop or partial calculations with a monochromatic beam can be used. SHADOW is also very powerful to study the focal spot dimensions as a function of the crystal shape. One can easily calculate systems with elliptical shapes that reduce the spherical aberrations. It is also possible to include in SHADOW a external mesh surface that may take into account surface errors. An optimization work for the ESRF dispersve EXAFS beamline including ray tracing calculations can be found in Ref. 27.

5.3. Sagittal bending

Many bending magnet beamlines equipped with a double crystal monochromator use sagittal bending of the second crystal to focus the synchrotron beam on the sample position. There are two important aspects of the sagittal focusing that can be studied with ray tracing. One is the beam transmission as a function of the accepted beam divergence and magnification factor; and the second is the quality of the focus. The latter is mainly due to the quality and alignment of the surface. The ideally cylindrical reflecting surface if often distorted by the effects of elastic bending, anticlastic[28] curvature, or artifacts left when suppressing anticlastic curvature, like deformations due

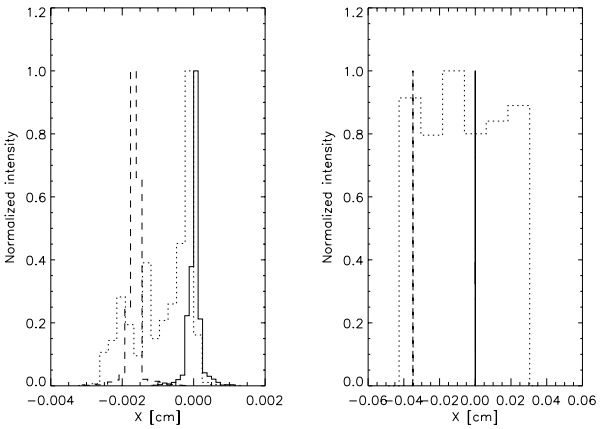

Figure 6. Beam cross section at the polychromatic focal plane (left) and at the monochromatic focal plane (right) for a $Si < 111 >$ asymmetric ($\alpha = -5^{\circ}$) bent (R=5.47 m) crystal reflecting at a nominal energy E_0=7111 eV. The source is at 40 m from the crystal and the polychromatic (monochromatic) focus is located at 1.00 m (1.30 m) downstream the crystal. The dotted histogram refers for an incident white beam whilst the continuos and dashed ones refer for monochromatic incident beam at energies of 7111 eV and 7211 eV, respectively. We observe that at the polychromatic focal plane the width of the polychromatic profile is narrower than in the monochromatic focal plane, but the inverse results for the monochromatic histograms.

to ribs. All of them can be treated with SHADOW, and the best way is to include a crystal profile either measured or calculated with finite element analysis.

In order to illustrate the suitability of SHADOW for studying sagitally focusing monochromators, we analyze the transmission of a sagittally bent monochromator as a function of the magnification factor. When focusing beams with divergences of several mrad, the sagittal bending of the second crystal produces a significant drop of the total transmitted intensity. This is done because when a ray arrives on the first crystal with an angle θ, it will impinge on the second with a different angle $\theta + \Delta\theta$. The error in the angle $\Delta\theta$ can be minimized, therefore maximazing the transmission, when a magnification $M = 1:3$ is chosen, as stated in Ref. 29 (see Fig. 7). Outside this magnification value, the transmission can be improved using conical (instead of cylindrical) surfaces.[30]

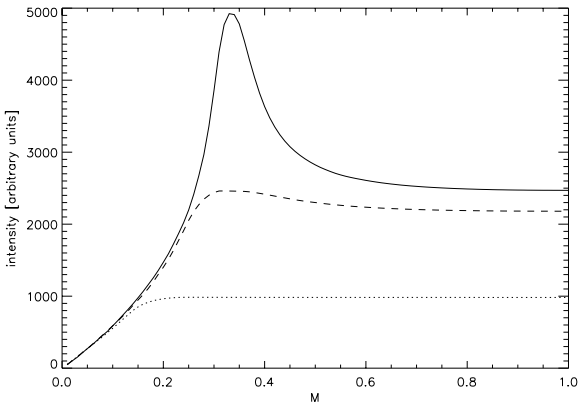

Figure 7. Intensity (in arbitrary units) versus magnification factor M for a point and monochromatic ($E = 20$ keV) source placed at 30 m from the sagittaly bent crystals. Three beam divergences are considered: 1 mrad (dotted), 2.5 mrad (dashed) and 5 mrad (continuous). We clearly observe the maximum of the transmission at M=0.33 when focusing the 5 mrad beam, as predicted by the theory.

5.4. Other systems

We have shown several examples of crystals system used in synchrotron radiation applications. There are many other crystal mountings that can be calculated with SHADOW and, although not very popular in synchrotrons, are quite useful in other research fields.

We developed a model[13] to perform ray tracing calculations for the Johansson[31] geometry. This geometry is used when it is necessary to focus a very divergent beam, and has many advantages respect to the usual bent crystal in Rowland geometry, also called Johann mounting. The idea is to produce a geometry in which both the geometrical focusing and the Bragg condition are satisfied along the crystal surface, condition which is not fulfilled in the Johann geometry. For that it is necessary to grind a crystal plate with a spherical shape of radius R and then bend the resulting surface to a radius $R/2 = R_{rowland}$. This is equivalent to introducing a local asymmetry cut in the crystal surface. In fact, SHADOW models this geometry by using a bent surface with an asymmetric cut which is dependent on the position in the surface, something like a variable ruling grating.

We also analyzed imaging properties of crystals by ray tracing. These crystals are often used for imaging x-ray plasma sources. A good spatial resolution (better than 4 μm) can be obtained by imaging an object with x-rays produced by the plasma source using a good quality spherical crystal. Experimental results and ray tracing calculations on these systems are studied in Ref. 32. Using these crystals and x-ray sources it is also possible to produce quasi-collimated beams (better than 1 mrad) as shown in Ref. 33.

6. NEW DEVELOPMENTS

Using the physical model described above, it would be possible to calculate many systems which are not presently available in SHADOW. A problem already addressed is the local change of reflectivity in elastically bent crystals due to deformation in the parallelism of the Bragg planes. It would be desirable (and work is in progress to implement it) to provide more general methods than the Zachariasen's one to do it. The possibility to use experimental diffraction profiles and rocking curves will also be very useful. Work is in progress to allow SHADOW to calculate any crystal structure (presently it includes six structures: ZincBlende, Rocksalt, simple FCC, CsCl, Hexagonal Close-Packed and Hexagonal Graphite). There are some crystal systems used in synchrotron radiation applications that use the transmitted and not the diffracted beam from crystals. Typical examples are the crystal polarizers, which could be easily implemented in SHADOW. It would also be easy to compute the penetration depth of the beam inside the crystal in perfect crystal by using a method similar to the one used for mosaic crystals.[5] This would be useful to study highly focusing systems. A model for crystals with low mosaicity going from the perfect crystal (mosaicity zero) to the mosaic crystal (mosaicity >> Darwin width) would also be useful for modeling real crystals.

It is possible with ray tracing to generate plane and spherical wavefronts and study its propagation. For such calculations *grid* sources should be used. A point and divergent source will produce a spherical wave front and an extended and collimated source simulates the plane wave. SHADOW can compute at each location the phase and it is possible (by writing some ad-hoc utilities) to reconstruct the wavefront after the optical elements.

6.1. Interference, diffraction and coherence

An important feature of SHADOW is that it calculates for any optical reflection the change in the electric field. It is possible to construct a mapping of the electric field at any location in the beamline, and to use this map as a source to calculate interference (by vector addition of the electric fields) and Fraunhofer or Fresnel diffraction (by solving the Fresnel-Kirchoff integral as done in the SHADOW's FFRESNEL utility). From the visibility of the diffraction patterns it is possible to study the coherence of the source and how the different optical elements alter this coherence. In Fig. 8a we have calculated the diffraction pattern produced by three slits (25, 12.5 and 5 μm) illuminated by a coherent monochromatic beam. The use of asymmetric crystals is quite delicate when using coherent beams because they reduce the transverse coherence length (due to the chromatic aberrations introduced[34]). In order to illustrate this phenomenon we have calculated the diffraction pattern produced by a coherent collimated beam for two cases: i) after diffraction by a symmetrical crystal, and ii) after diffraction by a slightly asymmetric $\alpha = 0.15^\circ$ crystal. In both cases two patterns are calculated for monochromatic sources, one for the nominal energy (E=8000.0 eV) and the second one for an energy of 8000.5 eV, which is inside the intrinsic resolution of the crystal ($\Delta E \approx 1$ eV). Results show that for the symmetrical case the two patterns are in phase, whereas for the asymmetrical case the patterns are out of phase. The observed pattern will be the addition of all the patterns for all the energies inside the energy

bandwidth of the crystals. Therefore, in the case of asymmetric crystals, the total diffraction pattern shows no visibility, thus destroying the spatial coherence, demonstrating that asymmetrical crystals destroy coherence because of the chromatic aberrations they produce.

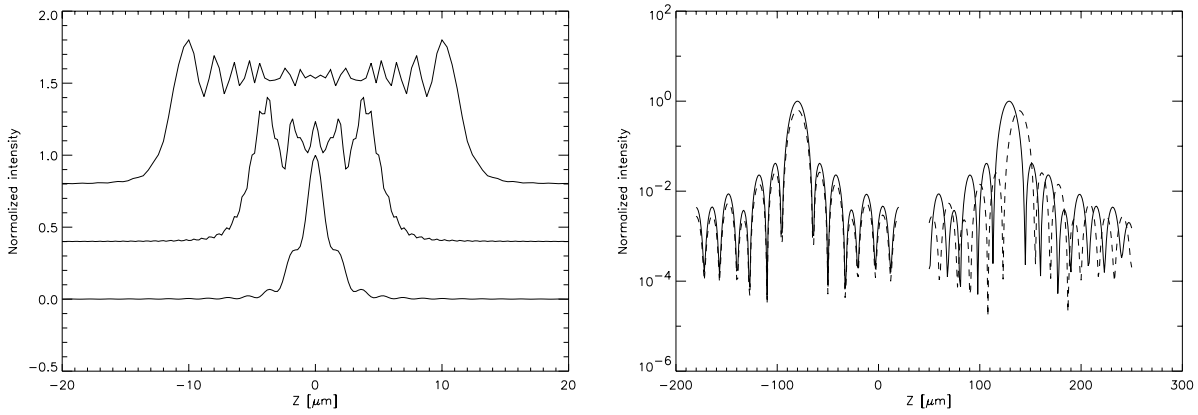

Figure 8. *Left:* Diffraction pattern (Fraunhofer diffraction) produced by a collimated coherent and monochromatic beam (E =8 keV) for three different slits of 25, 12.5 and 5 μm (from top to bottom). The diffraction patterns have been calculated using SHADOW at an image plate 10 cm downstream the slit. Plots have been shifted in vertical for clarity.
Right: Fraunhofer diffraction patterns produced by a collimated beam of 1 μm width, after diffraction by a symmetrical $Si < 1,1,1 >$ crystal (left curves) and an asymmetrical $\alpha = 0.15^\circ$ crystal (right curves). The continous lines correspond to beam energy of 8000.0 eV and the dashed ones to 8000.5 eV. Notice that the diffraction profiles in the asymmetrical case are shifted, as a result of the chromatic aberrations, destroying coherence. The symmetrical/asymmetrical plots have been shifted horizontally for clarity.

7. CONCLUSIONS

A high number of crystal devices used in x-ray technology can be simulated by using the ray tracing program SHADOW. We presented several examples of different instruments and devices extensively used in synchrotron radiation beamlines in order to demostrate its potential applicability. The calculated results were always benchmarked with either calculations using well established analytical formulas or related bibliography. These were only examples, and it is potentially possible to simulate an illimited number of devices presently in use or proposed for the future. The ray tracing method could also be used for calculations to study diffraction effects with partial coherent beams and the conservation and transfer of the coherence by the optical elements.

ACKNOWLEDGEMENT

Many thanks to Franco Cerrina (Center for X-ray Lithography, University of Wisconsin) for giving me the opportunity of developing with him the crystal models in SHADOW, which is in the base of the results presented in this and in many other papers.

REFERENCES

1. W. H. Zachariasen, *Theory of x-ray diffraction in crystals*, Dover, New York, 1994.
2. J. W. M. Du Mond, "Theory of the use of more than two successive x-ray crystal reflections to obtain increased resolving power," *Phys. Rev.* **52**, p. 872, 1937.
3. T. Matsushita and H.-O. Hashizume, *X-ray monochromators, in Handbook on Synchrotron Radiation (Ch 4), edited by E.E. Koch*, North-Holland, Amsterdam, 1983.
4. C. Welnak, G.J. Chen and F. Cerrina, "SHADOW: a synchrotron radiation and x-ray optics simulation tool," *Nucl. Instr. and Meth. in Phys. Res. A* **347**, pp. 344–347, 1994.

5. M. Sanchez del Rio, S. Bernstorff, A. Savoia and F. Cerrina, "A conceptual model for ray tracing calculations with mosaic crystals," *Rev. Sci. Instrum.* **63**, pp. 932–935, 1992.
6. M. Sanchez del Rio, M. Gambaccini, G. Pareschi, A. Taibi, A. Tuffanelli and A. Freund, "Focusing properties of mosaic crystals," *These proc.* , 1998.
7. Interactive Data Language (IDL) *by Research Systems Inc, 2995 Wilderness Place, Boulder, Colorado 80301* **http://www.rsinc.com**.
8. M. Sanchez del Rio and R.J. Dejus, "XOP: recent developments," *These proc.* , 1998.
9. M. Sanchez del Rio, C. Ferrero and V. Mocella, "Computer simulation of bent perfect crystal diffraction profiles," *Proc. SPIE* **3151**, pp. 312–323, 1997.
10. J.A.R. Samson, *Vacuum ultraviolet spectroscopy*, John Wiley, New York, 1967.
11. F.N. Chukhovskii and M. Krisch, "The lens equation for Bragg diffraction optics. The general case of asymmetric reflection," *J. Appl. Cryst.* **25**, pp. 211–213, 1992.
12. K. Takeshita, "Chromatic aberration of an asymmetrically cut curved crystal due to the dynamic diffraction effect," *Rev. Sci. Instrum.* **66**, pp. 2238–2240, 1995.
13. M. Sanchez del Rio and F. Cerrina, "Asymmetrically cut crystals for synchrotron radiation monochromators," *Rev. Sci. Instrum.* **63**, pp. 936–940, 1992.
14. M. Sanchez del Rio and A. Marcelli, "Waviness effects in ray-tracing of "real" opticsl surfaces," *Nucl. Instr. and Meth. in Phys. Res. A* **319**, pp. 170–177, 1992.
15. C. Masciovecchio, U. Bergmann, M. Krisch, G. Ruocco, F. Sette and R. Verbeni, "A perfect crystal X-ray analyser with meV energy resolution," *Nucl. Instr. and Meth. in Phys. Res. B* **111**, pp. 181–186, 1996.
16. R. Verbeni, F. Sette, M.H. Krisch, U. Bergmann, B. Gorges, C. Halcoussis, K. Martel, C. Masciovecchio, J.F. Ribois, G. Ruocco and H. Sinn, "X-ray monochromator with $2x10^{-8}$ energy resolution," *J. Synchrotron Rad.* **3**, pp. 62–64, 1996.
17. A. Caticha and S. Caticha-Ellis, "Dynamical theory of x-ray diffraction at Bragg angles near $\pi/2$," *Phys. Rev. B* **25**, pp. 971–983, 1982.
18. M. Deutsch, M. Hart and P. Sommer-Larsen, "Thermal motion of atoms in crystalline silicon: Beyond the debye theory," *Phys. Rev. B* **40**, pp. 11666–11669, 1989.
19. T. Ishikawa, Y. Yoda, K. Izumi, C.K. Suzuki, X.W. Zhang, M. Ando and S. Kituta, "Construction of a precision diffractometer for nuclear Bragg scattering at the Photon Factory," *Rev. Sci. Instrum.* **63**, pp. 1015–1018, 1992.
20. A. Chumakov, R. Rüffer, A.Q.R. Baron, J. Metge, H. Grünsteudel, H.F. Grünsteudel, "X-ray optics for nuclear inelastic scattering," *proc. SPIE* **3151**, pp. 262–270, 1997.
21. E.E. Alp, W. Sturhahn, T. Toellner, P. Lee, M. Schwoerer-Böhning, M. Hu, P. Hession, J. Sutter and P. Abbamonte, "Advances in high-energy-resolution x-ray scattering at beamline 3-ID," *Advanced Photon Source Research* **1**, pp. 9–14, 1998.
22. T. M. Mooney, T. Toellner, W. Sturhahn, E.E. Alp and S.D. Shastri, "High resolution, large-angular-acceptance monochromator for hard x rays," *Nucl. Instr. and Meth. in Phys. Res. A* **347**, pp. 348–351, 1994.
23. A.I. Chumakov, J. Metge, A.Q.R. Baron, H. Grünsteudel, H.F. Grünsteudel, R. Rüffer and T. Ishikawa, "An x-ray monochromator with 1.65 meV energy resolution," *Nucl. Instr. and Meth. in Phys. Res. A* **383**, pp. 642–644, 1996.
24. M. Sanchez del Rio, C. Ferrero, G-J. Chen and F. Cerrina , "Modeling perfect crystals in transmission geometry for synchrotron radiation monochromator design," *Nucl. Instr. and Meth. in Phys. Res. A* **347**, pp. 338–343, 1994.
25. M. Sanchez del Rio, G. Grübel, J. Als-Nielsen and M. Nielsen, "Focusing characteristics of diamond crystal x-ray monochromators. An experimental and theoretical comparison," *Rev. Sci. Instrum.* **66**, pp. 5148–5152, 1995.
26. M. Lemonnier, R. Fourme, F. Rousseaux and R. Kahn, "X-ray curved-crystal monochromator system at the storage ring DCI," *Nucl. Instr. and Meth.* **152**, pp. 173–177, 1978.
27. J. Pellicer-Porres, A. San Miguel and A. Fontaine, "High focussing Bragg polychromator design for energy dispersive x-absorption spectroscopy," *To be published in J. Synchrotron Rad* .
28. C.J. Sparks, G.E. Ice, J. Wong and B.W. Batterman, "Sagittal focusing of synchrotron x-radiation with curved crystals," *Nucl. Instr. and Meth.* **195**, pp. 73–78, 1982.

29. C.J. Sparks, B.S. Borie and J.B. Hastings, "X-ray monochromator geometry for focusing synchrotron radiation above 10 keV," *Nucl. Instr. and Meth.* **172**, pp. 237–242, 1980.
30. G.E. Ice and C.J. Sparks, "Conical geometry for sagittal focusing as applied to x rays from synchrotrons," *J. Opt. Soc. Am. A* **11**, pp. 1265–1271, 1994.
31. T. Johansson, "Uber ein neuartiges genau fokussierendes Rontgenspektrometer," *Z. Phys.* **82**, pp. 507–528, 1933.
32. M. Sanchez del Rio, A. Ya. Faenov, V.M. Dyakin, T.A. Pikuz, S.A. Pikuz, V.M. Romanova and T.A.Shelkovenko, "Ray-tracing for a monochromatic x-ray backlighting scheme based on spherically bent crystal," *Physica Scripta* **55**, pp. 735–740, 1997.
33. M. Sanchez del Rio, M. Fraenkel, A. Ziegler, A. Ya. Faenov and T.A. Pikuz, "A study of collimated x-ray beam formation by a femtosecond laser-produced plasma source using spherically bent crystals: ray-tracing simulations and experimental results," *Rev. Sci. Instrum. (submitted)* , 1998.
34. S. Brauer, G.B. Stephenson and M. Sutton, "Perfect crystals in the asymmetric Bragg geometry as optical elements for coherent x-ray beams," *J. Synchrotron Rad.* **2**, pp. 163–173, 1995.